# Chapter 11
# Magnetoresistance Effect

The history of the research on magnetoresistance effect is described first and then the basis of electron conduction is explained. Classification of the magnetoresistance effect is done. Among them, experiment on anisotropic magnetoresistance and its origin based on the model by Campbell et al. are explained. Further, it is shown that the measurement of magnetoresistance and magnetization curves is useful to investigate the magnetization states. Finally, the finding of giant magnetoresistance effect (GMR) and its further development are described.

## 11.1 History of research

The word "magneto-resistance" (magnetic resistance) is seen when we open a textbook to learn about electromagnetism. Here, the magnetic circuit may be considered to be corresponding to the electric circuit. Magnetoresistance is a value in which the magneto-motive force is divided by magnetic flux $N$ (product of the sectional area $S$ of the circuit and the magnetic flux density $B$). The magneto-motive force can be shown with $nI$. Here, $I$ is electric current in the coil that surrounds the magnetic circuit and $n$ is the number of wounded coils (Fig. 11.1b). The magnetoresistance in this case is proportional to the magnetic path length but inversely proportional to the product of permeability $\mu$ and the cross area $S$ of the material that composes the circuit. On the other hand, the explanations on magnetoresistance effect in this section on electric current magnetic effect (galvanomagnetic effect) are shown in the last pages of several technical books on magnetism. This is considered as an associated phenomenon of magnetization [1]. When the magnetic field is applied from the outside in this case, generically the phenomenon of the change of electric resistance of the material is called the magnetoresistance effect.

The research on the magnetoresistance effect is very old [2], and that on electromagnetism was completed as early as 1857. The anisotropic magnetoresistance effect (AMR) of the 3d transition metal and the alloy were researched by 1960 and

T. Miyazaki and H. M. Jin, *The Physics of Ferromagnetism*, Springer Series in Materials Science 158, DOI: 10.1007/978-3-642-25583-0_11,

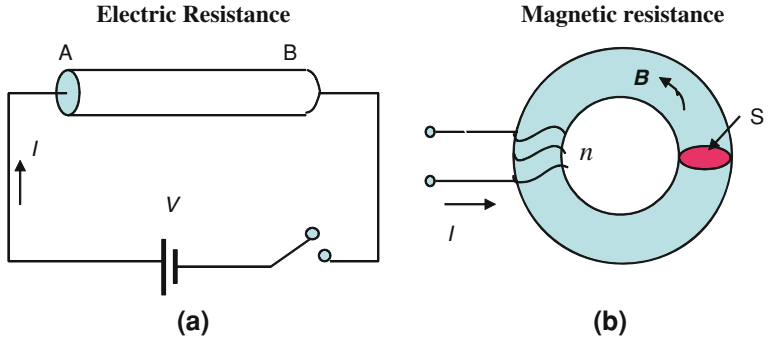


**Fig. 11.1** Comparison between electric resistance (**a**) and magnetic resistance (**b**). In the case of electric resistance $R_{AB}$, $V = IR_{AB}$, where $V$ is applied voltage, $I$ is current. While in the case of magnetic resistance $R_{AB}$, $F = NR_{AB}$, where $F$ is magnetomotive force and $N$ is magnetic flux. Here, $R_{AB}$ is given by $\oint dr/\mu S$, where $\mu$ is permeability and $S$ is a cross area of material

**Table 11.1** History of magnetoresistance effect research

| | |
|---|---|
| 1857 | Effects of magnetization on the electric conductivity of nickel and of iron, William Thomson, Proc. Roy. Soc. (London) 8(1857) 546–550 |
| 1930–1960 | Anisotropic magnetoresistance effect in 3d transition metal and alloys (AMR Effect) |
| 1960–1970 | AMR effect in metal and alloys and its interpretation (two current model, $\rho_\uparrow$, $\rho_\downarrow$). These are mainly carried out by Campbell and Fert |
| | Giant magnetoresistance effect in magnetic semiconductors ($CdCr_2Se_4 \cdots$) |
| 1975 | First report of related to tunnel magnetoresistance effect |
| See the following papers | |
| Anisotropic magnetoresistance in ferromagnetic 3d alloys, T. R. McGuire and R. I. Potter, IEEE Trans. Magn. MAG-11 (1975) 1018. | |
| Thin film magnetoresistors in memory, storage and related applications, D. A. Thompson et al., IEEE Trans. Magn. MAG-11 (1975) 1039 | |
| 1988 | Giant magnetoresistance in Fe/Cr super-lattices |

beyond [3]. Discussions based on the two current models to interpret the effect of AMR and GMR [4] of the magnetic semiconductor were researched in 1960–1970 [5]. The recent research on GMR and tunnel magnetoresistance effect (TMR) effect is the object of the artificial thin film or the junction, and the results achieved after a technological idea though a research was, in the past, the one intended for metals, alloys, or compounds. The historical details of the research on the magnetoresistance effect are roughly put together in Table 11.1. The root of TMR will be explained in detail in the Introduction of Chap. 12.

## 11.2 Basis of Electrical Conduction

The knowledge of the extent of thinning or reducing the thickness of a magnetic substance with a large resistivity to reduce the eddy current loss when the material was used in high frequency by the person who had been researching on magnetic materials. Therefore, there is not much knowledge of electrical conduction in general. Few experimental studies concerning magnetoresistance were done. Correspondingly, there are few reference books concerning conduction that become the basis as described in the previous section. Then, the author will explain some basic problems on conduction.

### *11.2.1 Drift Velocity and Fermi Velocity*

It is important to understand, at first, the terms Fermi velocity, relaxation time, and mean free paths when thinking about the conductivity of a material. If we do not understand these words and phrases, the behavior of the electron will not be well understood. Thus, the author first explains them though they are often described in textbooks. It is assumed that one electron is put in electric field $\boldsymbol{E}$.
Because the electron receives the power of $-e\boldsymbol{E}$, the movement is given by the following equation:

$$m\frac{\mathrm{d}^2\boldsymbol{r}}{\mathrm{d}t^2} = m\frac{\mathrm{d}\boldsymbol{v}}{\mathrm{d}t} = -e\boldsymbol{E}. \tag{11.1}$$

Here, $m$ is the mass of the electron and $-e$ the electric charge. Solving this equation, we have the relation $v = -(eE/t)t$, in which current density is expressed as $\boldsymbol{i} = n(-e)$. Hence,$\boldsymbol{v} = (ne^2\boldsymbol{E}/m)t$, which implies that the increase of electric current will increase with time. However, this behavior cannot be observed if the electric field is applied to an actual material, and the electric current shows the definite value only instantaneously. This is because the resistance force acts on the electron and the balance between them is maintained, becoming the constant speed. Let us assume resistance force is proportional to velocity, then the equation of motion is described as

$$m\frac{\mathrm{d}\boldsymbol{v}_D}{\mathrm{d}t} = -e\boldsymbol{E} + c\boldsymbol{v}_D. \tag{11.2}$$

It can be understood intuitively that this is the same as the motion equation of a raindrop that falls from the sky. We can describe $\boldsymbol{v_D}$ for the velocity in (11.2) because we treat the material as a many-electron system. It means the average velocity of the electron or drift velocity. Putting $c/m = -1/\tau$, ($\tau$: relaxation time), and solving (11.2), we have

$$\boldsymbol{v}_D = -\frac{e\tau}{m}\boldsymbol{E}. \tag{11.3}$$

where $\tau$ is the average time from the collision of the electron with the ion, etc., to the next collision. Equation (11.3) shows that the velocity of the electron (crowd) is proportional to the electric field, and the proportional coefficient $e\tau/m \equiv \mu$ depends on the following factors:

- Thermal motion of crystal lattice and ions.
- Defects such as grain boundary, dislocations, and voids in crystal.

For thin films, surface etc. cannot be disregarded. The electric current density is

$$\boldsymbol{i} = -ne\boldsymbol{v}_D = \frac{ne^2\tau}{m}\boldsymbol{E} \equiv \sigma \boldsymbol{E}. \tag{11.4}$$

Thus, we have

$$\sigma = \frac{ne^2\tau}{m}, \qquad \text{or} \qquad \rho = \frac{m}{ne^2\tau}. \tag{11.5}$$

Here, $n$ is the number of electrons per unit volume that contributes to conduction. The symbol $\sigma$ is called the rate of electric conductivity, and the reciprocal $\rho$ is called the resistivity or a specific resistance. If the value $\rho$ of the material is determined in (11.5), the relaxation time can be obtained. For instance, $\rho = 1.5\times10^{-8}\Omega$m, $n = 8.5 \times 10^{28}/\text{m}^3$, $e = 1.6 \times 10^{-19}$C, and $m = 9.1 \times 10^{-31}$ kg in Cu, thus, $\tau = 3.8 \times 10^{-14}$ s. By the way, the movement of the electron when the electric field is applied to the material has been described till now. When the electric field is not applied, are the electrons in a stationary state? To tell the truth, the electron does a random movement even though the electric field is not applied. The density of states is used to describe the energy state of the electron. The electrons are packed from the lowest energy state, to the highest energy level, so-called Fermi level. When we assume the Fermi energy ( see Fig. 11.2) at the speed of the electron that exists in the Fermi level to be $E_F$, it can be shown as

$$\frac{1}{2}mv_F^2 = E_F. \tag{11.6}$$

For instance, in $E_F = 7\,\text{eV}$ ($7 \times 1.6 \times 10^{-19}$J) of Cu it becomes $v_F = 1.3 \times 10^6$ m/s ($= 470 \times 10^4$ km/h), and is $10^4$ times further as fast as the fastest train developing in the world now. By the way, when the distance between the collision (scatter) and the next collision is assumed to be $\ell$, we have $\ell = 350$ Å from $\ell = v_F \cdot \tau$. The length $\ell$ is called the mean free path of the electron. Drift velocity previously described becomes $v_D = 5$ mm/sec, assuming $E = 1$ V/m and is far smaller compared with $v_F$. The movements of the particles (water molecules) are violent and random in volcanic smoke that occurs from a volcano. The velocity corresponds to the Fermi ones. The entire volcanic smoke will move sideways if the wind blows from the side against this volcanic smoke. We are able to understand intuitively that this is one-sided velocity.

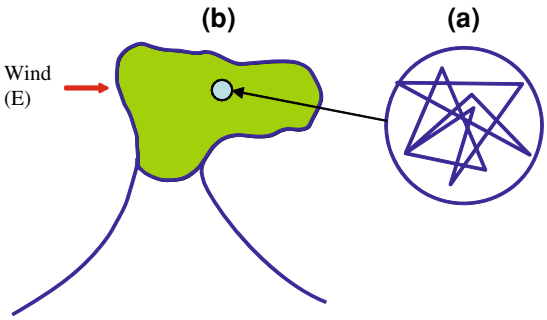


**Fig. 11.2** Scheme for intuitive understanding both **a** Fermi velocity and **b** drift velocity

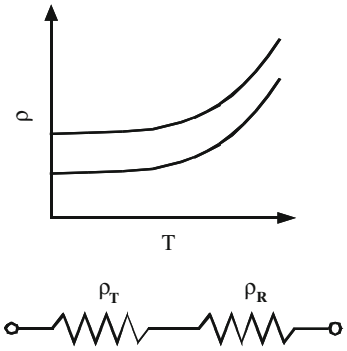


**Fig. 11.3** Matthiessen's law, $\rho_R$, $\rho_T$ are the resistivities due to impurity and phonons, respectively

### *11.2.2 Matthiessen's Law*

There are two kinds of $1/\tau$, if there are two factors for scattering of the electrons. Thus, the rate of resistance is given by

$$\rho = \frac{m}{ne^2}\left(\frac{1}{\tau_1} + \frac{1}{\tau_2}\right) = \rho_1 + \rho_2. \tag{11.7}$$

For instance, two kinds of scattering may be considered to be caused from impurities and lattice vibrations ($\rho_T$). Thus, we have the resistivity as $\rho = \rho_R + \rho_T$. The total resistance is shown by the sum of $\rho_R$ and $\rho_T$ of individual resistance, which is called Matthiessen's law. Figure 11.3 shows this law schematically $\rho_R$.

### *11.2.3 Two-Current Model*

How can we observe phenomena that in the kind of medium where the electron moves in case of the above-mentioned, etc., two kinds of scattered ones (electron) exist? These cannot be distinguished, because $e$ is an elementary charge and any

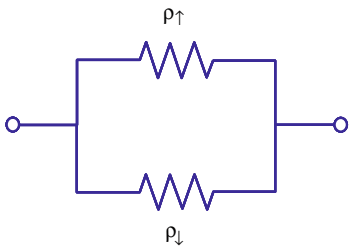


**Fig. 11.4** Two-current model, $\rho_\uparrow$ and $\rho_\downarrow$ are the resistivities of $\uparrow$ and $\downarrow$ electrons, respectively

electron is the same as the mass in $m$, even if two kinds of electrons are assumed. However, two kinds of electrons with different spins may be considered because there are electrons of $\uparrow$ (up spin) and $\downarrow$ (down spin) in the ferromagnetic substance. That is, we can consider about the two kinds of relaxation times, and assume both the electron numbers to be equal. Then, we have (11.8) as follows:

$$\sigma = \frac{ne^2}{m}(\tau_\uparrow + \tau_\downarrow) = \sigma_\uparrow + \sigma_\downarrow \quad \text{or} \quad \rho = \frac{\rho_\uparrow \rho_\downarrow}{\rho_1 + \rho_2} \tag{11.8}$$

That is, the equivalent circuit is shown as in Fig. 11.4.

### *11.2.4 Resistance Due to Spin Flip*

It was considered that the spins of $\uparrow$ and $\downarrow$ are maintained in the case of scattering in the current discussion. That is, the scattering by the magnon or the phonon can be disregarded at low temperature [6, 7]. Then, how does it occur with rising temperature? It is thought that the change (spin flip) in $\uparrow \leftrightarrow \downarrow$ occurs because of scattering by the magnon and the spin flip because of the phonon, even though the extent is small. How can the resistance for that case be shown? Figure 11.5 shows this model schematically.

The rate of a decrease in the momentum is a product of the change in the scattering probability and the momentum. Since $d\boldsymbol{p}/dt = \boldsymbol{F}$,

for the spin $\uparrow$,

$$-eE = \frac{1}{\tau_\uparrow} m v_\uparrow + \frac{1}{\tau_{\uparrow\downarrow}} m(v_\uparrow - v_\downarrow).$$

For $\downarrow$ spin,

$$-eE = \frac{1}{\tau_\downarrow} m v_\downarrow + \frac{1}{\tau_{\downarrow\uparrow}} m(v_\downarrow - v_\uparrow). \tag{11.9}$$

It is assumed here that $\tau_{\uparrow\downarrow}$ and $\tau_{\downarrow\uparrow}$ are equal. Each of $\uparrow$ and $\downarrow$ spins,

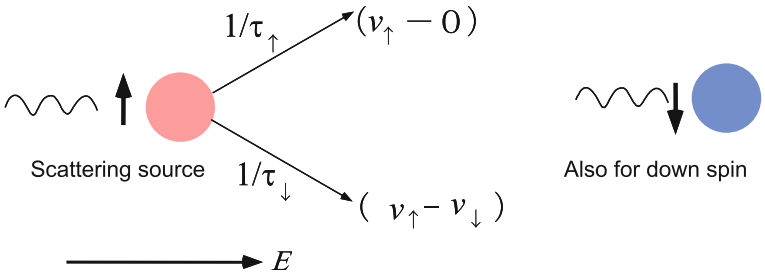


**Fig. 11.5** In the model chart, each of $\tau_\uparrow$ and $\tau_\downarrow$ is relaxation time, while spin flip occurs, each of $v_\uparrow$ and $v_\downarrow$ is corresponding to each velocity

$$i_{\uparrow(\downarrow)} = nev_{\uparrow(\downarrow)}, \quad \rho = m/ne^2\tau_{\uparrow(\downarrow)}, \tag{11.10}$$

then,

$$\frac{1}{\tau_\uparrow} = \frac{ne^2}{m}\rho_\uparrow = \frac{ne^2}{m}\left[\rho_\uparrow(0) + \rho'_\uparrow(T)\right]. \tag{11.11}$$

Here, $\rho_\uparrow(T)$ is an increment of resistance with the temperature. That is, it is resistance by an electronic phonon scattering. Similarly,

$$\frac{1}{\tau_\downarrow} = \frac{ne^2}{m}\rho_\downarrow = \frac{ne^2}{m}\left[\rho_\downarrow(0) + \rho'_\downarrow(T)\right]. \tag{11.12}$$

In addition,

$$\rho_{\uparrow\downarrow}(T) = \frac{m}{ne^2\tau_{\uparrow\downarrow}}. \tag{11.13}$$

Therefore, resistance at temperature $T$ is given by

$$\rho(T) = \frac{E}{i_\uparrow + i_\downarrow} = \frac{E}{ne} \cdot \frac{1}{v_\uparrow + v_\downarrow} \tag{11.14}$$

First obtaining $v_\uparrow$ and $v_\downarrow$ from (11.9), next substituting them into (11.14) and finally using (11.11–11.13),

$$\rho(T) = \frac{\left[\rho_\uparrow(0) + \rho'_\uparrow(T)\right]\left[\rho_\downarrow(0) + \rho'_\downarrow(T)\right] + \rho_{\uparrow\downarrow}(T)\left[\rho_\downarrow(0) + \rho_\uparrow(0) + \rho'_\uparrow(T) + \rho'_\downarrow(T)\right]}{\rho_\downarrow(0) + \rho_\uparrow(0) + \rho'_\uparrow(T) + \rho'_\downarrow(T) + 4\rho_{\uparrow\downarrow}(T)} \tag{11.15}$$

In the special case of scattering, let us consider that the spin flip by the magnon scattering occurs but the scattering by the phonon can be disregarded. From (11.15),

$$\rho = \frac{\rho_\uparrow \rho_\downarrow + \rho_{\uparrow\downarrow}(\rho_\uparrow + \rho_\downarrow)}{\rho_\uparrow + \rho_\downarrow + 4\rho_{\uparrow\downarrow}}. \tag{11.16}$$

We can see the representation often in such published papers as Fert et al. [7] published.

### *11.2.5 Temperature Dependence of ρ*

In (11.7), $\rho_\uparrow(0), \rho_\downarrow(0) \gg \rho'_\uparrow(T), \rho'_\downarrow(T), \rho'_{\uparrow\downarrow}(T)$ and $\rho'_\uparrow(T) = \rho'_\downarrow(T) \equiv \rho'_i(T)$ $(i = \uparrow, \downarrow)$, further we put $\rho_\uparrow(0) = a$, $\rho_\downarrow(0) = b$, $\rho_i(T) = c$, $\rho_{\uparrow\downarrow}(T) = d$, Then, (11.16) is expressed as

$$\begin{aligned}\rho &= \frac{(a+b)(b+c) + d(a+b+2c)}{a+b+2c+4d} \\ &= \frac{1}{a+b}\left[\{ab + c(a+b) + d(a+b+2c)\}\left\{1 - \frac{4(c+d)}{a+b}\right\}\right] \\ &\approx \frac{ab}{a+b} + \frac{(a-b)^2}{(a+b)^2}c + \frac{(a-b)^2}{(a+b)^2}d,\end{aligned} \tag{11.17}$$

$$\rho(T) = \frac{\rho_\uparrow(0)\rho_\downarrow(0)}{\rho_\uparrow(0) + \rho_\downarrow(0)} + \left[\frac{\rho_\uparrow(0) - \rho_\downarrow(0)}{\rho_\uparrow(0) + \rho_\downarrow(0)}\right]^2 \rho_i(T) + \left[\frac{\rho_\uparrow(0) - \rho_\downarrow(0)}{\rho_\uparrow(0) + \rho_\downarrow(0)}\right]^2 \rho_{\uparrow\downarrow}(T). \tag{11.18}$$

If the relations are set in Fert's article as follows:

$$\frac{\rho_\downarrow(0)}{\rho_\uparrow(0)} \equiv \alpha, \quad \frac{\rho_\uparrow(0)\rho_\downarrow(0)}{\rho_\uparrow(0) + \rho_\downarrow(0)} \equiv \rho_0$$

the following relation is introduced:

$$\rho(T) = \rho_0 + \left[\frac{\alpha - 1}{\alpha + 1}\right]^2 \rho_i(T) + \left[\frac{\alpha - 1}{\alpha + 1}\right]^2 \rho_{\uparrow\downarrow}(T). \tag{11.19}$$

Here, $(\alpha - 1)^2 / (\alpha + 1)^2$ is independent of the temperature, which is, however, determined by $\rho_\uparrow(0)$ and$\rho_\downarrow(0)$. Moreover, the first term of (11.19) corresponds to the residual resistivity, and the second and third terms to the scattering by the phonon and the magnon (the gap from the Matthiessen's law).

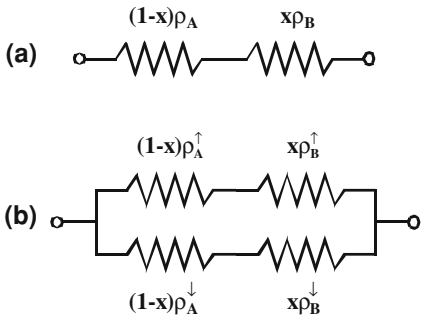


**Fig. 11.6** **a** Matthiessen's law and **b** two-current model in $A_{1-x}B_x$ alloy

### *11.2.6 How to Obtain $\rho_\uparrow$, $\rho_\downarrow$, and $\alpha = \rho_\downarrow/\rho_\uparrow$*

The author explains how to obtain $\rho_\uparrow$ and $\rho_\downarrow$ next, following the points of an argument in papers such as Fert and Campbell [8, 9]. The resistance of the $MA_{1-x}B_x$ alloy will be discussed. It is assumed either of magnetic elements of M such as Fe, Co, and Ni here, and A and B are the 3d transition metal elements other than Ni such as Fe, Co, Mn, Cr, and V. Resistance (residual resistivity) is expressed as

$$\rho_1 = \rho_0 + (1-x)\rho_A + x\rho_B, \tag{11.20}$$

when a resistance changes according to Matthiessen's law (Fig. 11.6a).
where, $\rho_0$ is s resistivity without A and B elements and $\rho_A$ and $\rho_B$ are resistivity per atom for A and B elements, respectively. On the other hand, $\uparrow$ and $\downarrow$ spins become parallel connection in two-current model as shown in Fig. 11.6b. That is, the total resistance is given by

$$\rho_2 = \rho_0 + \frac{\left[(1-x)\rho_A^\uparrow + x\rho_B^\uparrow\right]\left[(1-x)\rho_A^\downarrow + x\rho_B^\downarrow\right]}{(1-x)\rho_A^\uparrow + x\rho_B^\uparrow + (1-x)\rho_A^\downarrow + x\rho_B^\downarrow}, \tag{11.21}$$

$$\Delta\rho = \rho_2 - \rho_1 = \frac{(\alpha_A - \alpha_B)^2(1-x)\rho_A x\rho_B}{(1+\alpha_A)^2\alpha_B(1-x)\rho_A + (1+\alpha_B)^2\alpha_A x\rho_B}, \tag{11.22}$$

where,

$$\rho_A = \frac{\rho_A^\uparrow\rho_A^\downarrow}{\rho_A^\uparrow + \rho_A^\downarrow}, \quad \rho_B = \frac{\rho_B^\uparrow\rho_B^\downarrow}{\rho_B^\uparrow + \rho_B^\downarrow} \tag{11.23}$$

$$\alpha_A \equiv \frac{\rho_A^\downarrow}{\rho_A^\uparrow}, \quad \alpha_B \equiv \frac{\rho_B^\downarrow}{\rho_B^\uparrow} \tag{11.24}$$

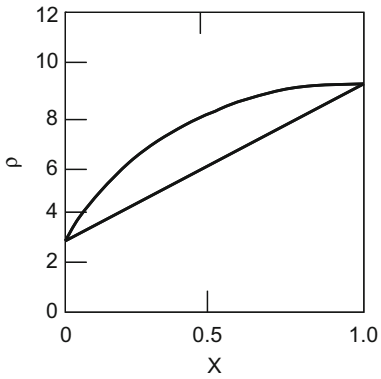


**Fig. 11.7** Residual resistivity of $MA_{1-x}B_x$ alloys (schematic). The two-current model in the curved line and the Matthiessen's law in the straight line are shown, respectively

or,

$$\rho_A^{\uparrow} = \frac{(1+\alpha_A)}{\alpha_A}\rho_A, \quad \rho_A^{\downarrow} = (1+\alpha_A)\rho_A \tag{11.25}$$

$$\rho_B^{\uparrow} = \frac{(1+\alpha_B)}{\alpha_B}\rho_B, \quad \rho_B^{\downarrow} = (1+\alpha_B)\rho_B. \tag{11.26}$$

Here, $\alpha_{A(B)}$ is an important value to discuss the magnetoresistance, so the concrete example will be shown later. The ratio of $\rho_{\downarrow}$ to $\rho_{\uparrow}$ is physically significant but not only parameter though some persons call it parameter $\alpha$. For $\alpha_{A(B)}$, the following experiments only have to be analyzed. First of all, residual resistivity $\rho_{A(B)}$ $(\mu\Omega \cdot cm/at\%)$ is necessary to obtain from the experiment on the electric resistance of dual alloy MA(B) that puts the A(B) atom, respectively, as impurities in M. Next, the residual resistivity of the ternary alloy $MA_{1-x}B_x$ is measured. In general, one data (curved line) may be obtained as shown in Fig. 11.7. From this data, $\rho_2 - \rho_1$ may be obtained. Equation (11.22) is best fitted to the experimental value of $\rho_2 - \rho_1$. From (11.22), the following are obtained:

$$\frac{1}{a} \cdot \frac{\Delta\rho}{\rho_B x} + \frac{1}{b} \cdot \frac{\Delta\rho}{\rho_A(1-x)} = 1 \tag{11.27}$$

$$a = (\alpha_A - \alpha_B)^2 / (1+\alpha_A)^2 \alpha_B.$$

$$b = (\alpha_A - \alpha_B)^2 / (1+\alpha_B)^2 \alpha_A \tag{11.28}$$

Therefore, we have a straight line when $\Delta\ \rho/\rho_B x$ is plotted with respect to $\Delta\rho/\rho_A\ (1-x)$ and then $\alpha$ may be obtained from the intersection of the axis with the straight line. This value is substituted into (11.28), and we can solve these equations

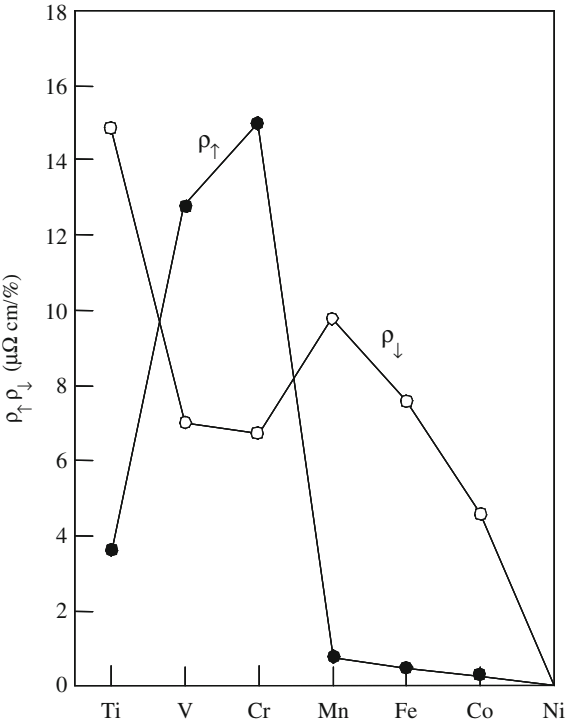


**Fig. 11.8** Values of $\rho_\uparrow$ and $\rho_\downarrow$ put in various 3d impurities of Ni

simultaneously with respect to $\alpha_A$ and $\alpha_B$. If $\alpha_{A(B)}$ is obtained, $\rho^{\uparrow}_{A(B)}$ from (11.25), $\rho^{\downarrow}_{A(B)}$ from (11.24). Figure 11.8 shows the value of $\rho^{\uparrow}_{A}$, $\rho^{\downarrow}_{A}$ to examine the ternary alloy with M = Ni (A or B = Co, Fe, Mn, Cr, V, and Ti).

## 11.3 Classification of Magnetoresistance Effects

The phenomenon of the change of conductivity by the applied magnetic field is generically called a magnetoresistance effect. The contents are divided into the variable case. The resistivity changes even if the magnetic field is applied not to the ferromagnetic substance but to the non-magnetic substance. This is called ordinary magnetoresistance effect. The lower the temperature, the stronger the magnetic field, and the more remarkable the effect. On the other hand, the magnetic field is applied to the material that has spontaneous magnetization, the ferromagnetic substance, and the phenomenon of the change of resistivity, corresponding to the magnetized state, is called anomalous magnetoresistance effect. The change of resistivity in ferromagnetic films such as Permalloy often examined depends on the direction of the spontaneous magnetization. These are called anisotropic magnetoresistance

**Table 11.2** Classification of magnetoresistance effects

| |
|---|
| (1) Nomal magnetoresistance effect |
| (2) Effect of anomalous magnetoresistance |
| (i) Anisotropic magnetoresistance effect (orientation effect) |
| (ii) Giant magnetoresistance effect (The spin valve is included) |
| (iii) Tunnel magnetoresistance effect |
| (iv) Forced magnetoresistance effect |

(AMR effect) or orientation effect. The multilayered thin film that repeats the metallic lattice or this accumulates of F/N/F is as described in Sect. 5.2. In the case, a negative exchange interaction works at interface of ferromagnetic layer. As a result, the magnetization is in the state of the antiparallel. In this case, the magnetic field is applied so that the magnetization can be in a parallel state and then, the resistance decreases. Because the ratio of changes is larger than AMR, this effect is called a GMR effect. Moreover, the change of tunneling current depends on a relative angle of the magnetization of both ferromagnetic substances between which the insulator is inserted. This is called a TMR effect. In both the GMR effect and the TMR effect, the change of resistivity may be observed depending on the relative angle of the magnetization of the ferromagnetic layers. In the former, there are two types of situations in the directions of current. One is the case of the parallel electric current in plane (CIP) and the other is perpendicular to the accumulating side, or current perpendicular to plane (CPP).

However, only CPP is in the TMR. Details of GMR and the effect of TMR will be mentioned in Sect. 11.7 and Chap. 12, respectively. In addition, there is an effect of the Perovskite type Mn oxide described for a super huge magnetoresistance (Colossal magnetoresistance: CMR for short), too. The magnetoresistance effect is brought together above, as shown in Table 11.2.

## 11.4 Anisotropic Magnetoresistance Effect

Let us consider the physical meaning of $\alpha$ that implies the degree of the spin-dependent condition. Here, $\alpha$ is defined as $\alpha_{\downarrow}/\alpha_{\uparrow}$. So, the equation $\alpha = 1$ means that $\rho_{\uparrow}$ and $\rho_{\downarrow}$ are equal, and the resistivity is equal in $\uparrow$ and $\downarrow$ electrons. That is, there is no scattering depending on a spin. Therefore, the magnetoresistance effect does not occur for this case. In contrast, the scattering depending on the spin may be remarkable in the case $\alpha \gg 1$ or $\alpha \ll 1$. That is, the GMR is sure to appear. Let us think how it is possible to show by the magnetoresistance effects using $\alpha$ of the effect of AMR. Figure 11.9 shows one example of the magnetoresistance curve of the Permalloy thin film. The $\rho_{//}$ shows the specific resistance when the magnetic field is applied in the same direction as the electric current and $\rho_{\perp}$ in the perpendicular situation. The magnetoresistance ratio is defined as

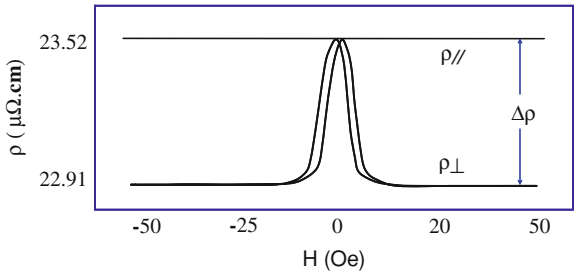


**Fig. 11.9** Magnetoresistance curve of permalloy thin film

$$\frac{\Delta\rho}{\rho_0} = \frac{\rho_{//} - \rho_\perp}{\frac{1}{3}\rho_{//} + \frac{2}{3}\rho_\perp} \times 100 \approx \frac{\rho_{//} - \rho_\perp}{\rho_\perp} \times 100 \approx \frac{\rho_{//} - \rho_\perp}{\rho_{//}} \times 100, \tag{11.29}$$

where $\rho_0$ is a resistivity ratio in the demagnetized state, and may be shown by using $\rho_{//}$ and $\rho_\perp$ like in (11.29). The approximation may be supported by the justification that $\rho_{//} \approx \rho_\perp$, since$\rho_{//}$ and $\rho_\perp$ are resistivities with ↑ and ↓ electrons, respectively.

$$\rho_{//(\perp)} = \frac{\rho^{\uparrow}_{//(\perp)}\rho^{\downarrow}_{//(\perp)}}{\rho^{\uparrow}_{//(\perp)} + \rho^{\downarrow}_{//(\perp)}}. \tag{11.30}$$

Further, $\rho^{\uparrow}_{//}$ is not independent of $\rho^{\uparrow}_{\perp}$ and also $\rho^{\downarrow}_{//}$ is not independent of $\rho^{\downarrow}_{\perp}$, and the following relations are led:

$$\rho^{\uparrow}_{//} = \rho^{\uparrow}_{\perp} + \gamma\rho^{\downarrow}_{\perp},$$

$$\rho^{\downarrow}_{//} = \rho^{\downarrow}_{\perp} - \gamma\rho^{\downarrow}_{\perp}. \tag{11.31}$$

Leading (11.31) is a little troublesome exercise level of quantum mechanics which the author will explain in the next section.

In these equations, $\gamma = (\lambda/H_{\mathrm{ex}})^2$ and $\lambda$ is spin-orbital interaction coefficient and $H_{\mathrm{ex}}$ is exchange interaction energy. In Fe, Ni, Co, and the alloys, $\gamma$ is of the order of 0.01. When we transform (11.29) by using (11.30) and (11.31),

$$\frac{\Delta\rho}{\rho_0} = (1 + \alpha\gamma)(1 - \gamma) - 1 \approx \gamma(\alpha - 1), \tag{11.32}$$

where $\alpha \equiv \rho^{\downarrow}_{\perp}/\rho^{\uparrow}_{\perp}$. It is understood to satisfy (11.32) though the arranged experimental results of $\alpha$ are shown in Fig. 11.10. The first report of the AMR was in the 1800s. However, the effect has been in the spotlight since the latter half of the 1980s. The recording density of the hard disk went up, and the tendency to use the

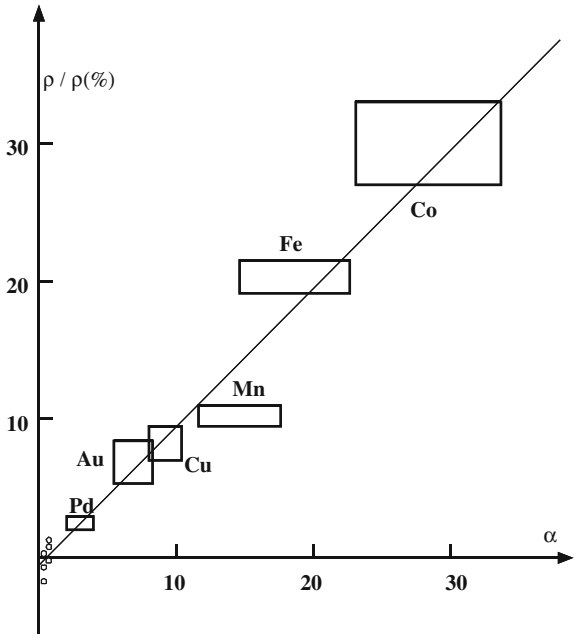


**Fig. 11.10** $\alpha = \rho_{\downarrow}/\rho_{\uparrow}$ dependence compared with AMR when various 3d impurities are introduced in Ni. The straight line shows $\Delta\rho/\rho_0 = 0.01\,(\alpha - 1)$

magnetoresistance effect as a magnetic head of high sensitivity was on the rise. The composition dependence of Ni–Fe–Co ternary alloy films (chemical composition) is shown in Fig. 11.11 [10, 11].

At 7 % Fe and 10–20 %Co of chemical composition, $\Delta\rho/\rho_0$ is understood to indicate the large value. Calculating the composition dependence of the $\alpha$ of Ni–Fe–Co referring to the discussion about the above-mentioned behavior, we show the result in the contour line in Fig. 11.12. In this case, we have the value of $\alpha$ using the value estimated by the proportion distribution in the bulk value of Ni–Fe and Ni–Co. When Figs. 11.11 and 11.12 are compared, it is understood that the composition dependence of $\alpha$ is almost corresponding to that of $\Delta\rho/\rho_0$.

## 11.5 Origin of Anisotropic Magnetoresistance Effect

Why is the AMR caused? It is not a phenomenon intuitively understood easily [12]. Thus, the author explains how the relation of (11.31) of the previous section is to be derived.

Resistivity is given by

$$\rho = \frac{m}{ne^2}\frac{1}{\tau}, \tag{11.33}$$

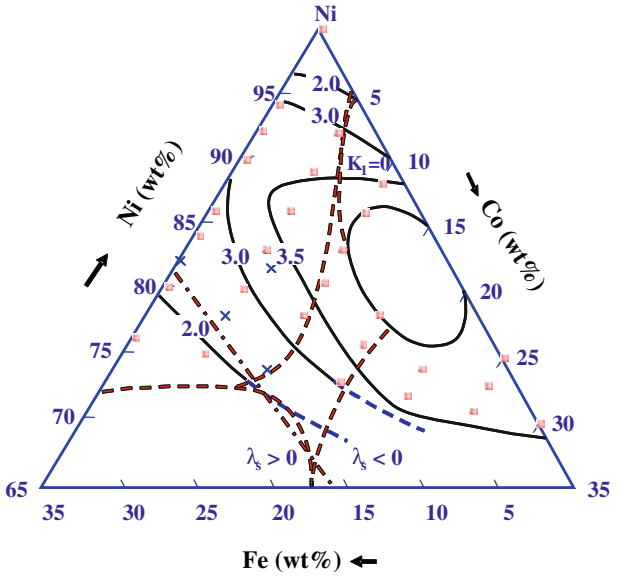


**Fig. 11.11** Composition dependence of MR ratio of Ni–Fe–Co ternary alloy thin film

though the author has already discussed the resistivity in Sect. 11.2, where $\tau$ is a relaxation time and $1/\tau$ shows the probability of the electron scattering. It is assumed that the electron of the wave of $\Psi_1$ is scattered by potential $V(r)$ and changed to the wave of $\Psi_2$. $1/\tau$ is given by

$$\frac{1}{\tau} \propto \left| \int \Psi_2^* V(r) \Psi_1 dv \right|^2 . \tag{11.34}$$

The discussion will be in more detail about Ni now. In view of the electronic structure of Ni, leading parts of conduction are 4s electrons. However, the anisotropy does not come out, taking considerations only to 4s electrons. If the scheme of scattering may be expressed concretely in consideration of this, it becomes as shown in Fig. 11.13. Assuming that $\Psi_s$ and $\Psi_d$ are electron wave functions in $s$ and $d$ states, respectively, and that the spin flip may not be occurred by the spin scattering, the transition of the electron from 1 to 2 is

$$\int \Psi_s^{*\uparrow} V(r) \Psi_s^{\uparrow} dv \tag{11.35}$$

$$\int \Psi_d^{*\uparrow} V(r) \Psi_s^{\uparrow} dv \tag{11.36}$$

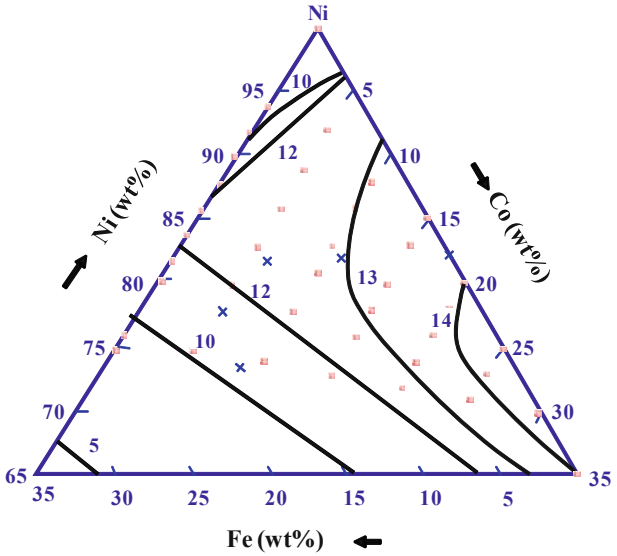


**Fig. 11.12** Composition dependence of $\alpha\left(\rho_{\downarrow}/\rho_{\uparrow}\right)$ of Ni–Fe–Co ternary alloy thin film

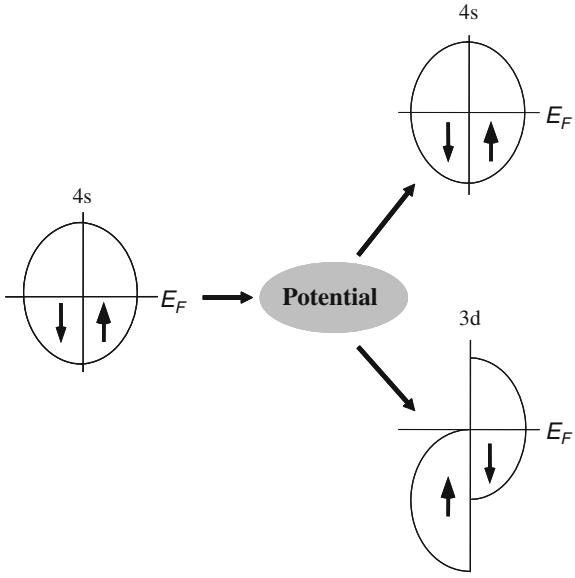


**Fig. 11.13** Scattering process and $1/\tau$ of 4s electrons are given

$$\int \Psi_s^{*\downarrow} V(r) \Psi_s^{\downarrow} dv \tag{11.37}$$

$$\int \Psi_d^{*\downarrow} V(r) \Psi_s^{\downarrow} dv. \tag{11.38}$$

Four transitions described above may be considered. However, neither (11.35) nor (11.37) (with transition from $s$ to $s$) contributes to the AMR. Moreover, the transition (11.36), $s^{\uparrow} \rightarrow d^{\uparrow}$ vanishes, since there is no density of state $\uparrow$ at the Fermi energy, as shown in Fig. 11.13. After all, we only have to consider the transition of $s^{\downarrow} \Rightarrow d^{\downarrow}$ in (11.38). When the plane wave is assumed to be $\Psi_s^{\downarrow} = e^{i\boldsymbol{k}\cdot\boldsymbol{r}}$, the normal state of the $d$ electron is described by five wave functions of $\ell = 2$, m $= 2, 1, 0, -1,$ and $-2$. It is assumed that the $\Psi$ of (11.38) is a product of the orbit and the spin here and the part in the orbit is in the form of the variable separation. Thus we have

$$\lambda L \cdot S\Psi \,|2\downarrow\rangle = \left(1 - \frac{1}{2}\varepsilon^2\right)\phi \,|2\downarrow\rangle + \varepsilon\phi \,|1\uparrow\rangle \tag{11.39}$$

$$\lambda L \cdot S\Psi \,|1\downarrow\rangle = \left(1 + \frac{3}{4}\varepsilon^2\right)\phi \,|1\downarrow\rangle + \left(\frac{3}{2}\right)^{1/2} \varepsilon\phi \,|0\uparrow\rangle \tag{11.40}$$

$$\lambda L \cdot S\Psi \,|0\downarrow\rangle = \left(1 - \frac{3}{4}\varepsilon^2\right)\phi \,|0\downarrow\rangle + \left(\frac{3}{2}\right)^{1/2} \varepsilon\phi \,|-1\uparrow\rangle \tag{11.41}$$

$$\lambda L \cdot S\Psi \,|-1\downarrow\rangle = \left(1 - \frac{1}{2}\varepsilon^2\right)\phi \,|-1\downarrow\rangle + \varepsilon\phi \,|-2\uparrow\rangle \tag{11.42}$$

$$\lambda L \cdot S\Psi \,|-2\downarrow\rangle = \phi \,|-2\downarrow\rangle\,. \tag{11.43}$$

Here, $\varepsilon = \lambda / H_{\mathrm{ex}}$. In (11.38), $\Psi_d^{\downarrow}$ is expressed by the product of orbit and spin ($\chi$). Further, the orbital part is expressed by the product of functions $R_{n\ell}(r)$ and $\phi_{\ell}^{n}$.

$$\Psi_d^{\downarrow} = R_{n\ell}(r)\phi_{\ell}^{m} \cdot \chi. \tag{11.44}$$

Here, $n, \ell, m$ are principal, azimuth, and magnetic quantum numbers, respectively and in this case $n = 3$, $m = \pm 2, \pm 1, 0$. Therefore, $\phi_2^m$ is given by

$$m = \pm 2 \qquad \phi_2^{\pm 2} \propto \frac{1}{2\sqrt{2}}(x \pm iy)^2 \tag{11.45}$$

$$m = \pm 1 \qquad \phi_2^{\pm 1} \propto \mp\frac{1}{\sqrt{2}} z\,(x \pm iy) \tag{11.46}$$

$$m = 0 \qquad \phi_2^{0} \propto \frac{1}{2\sqrt{3}}(r^2 - 3z^2). \tag{11.47}$$

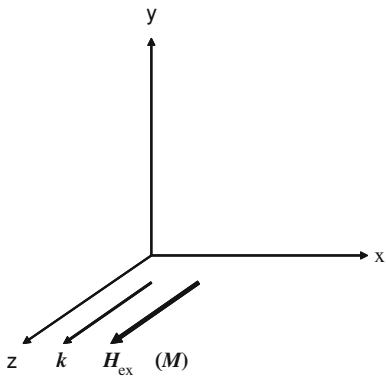


**Fig. 11.14** Wave number of electron and relation to external magnetic field

We choose the coordinate system as shown in Fig. 11.14 and discuss for two cases. ① $\boldsymbol{k} = (0, 0, k_z)$ case. This corresponds to the electric current that is parallel to magnetization, namely corresponding to $\rho_{//}$. In (11.33), $\rho$ is divided by $m/ne^2$ and put as $\rho$.

$$\rho_{\mathrm{sd}}^{\uparrow}(k_z) = \left| \int \left[ \mathrm{sum.of.right.side} \cdot \mathrm{term} \cdot \mathrm{in} \cdot (11.39) - (11.42) \right] * V(r) e^{ik_z z} dv \right|^2 \tag{11.48}$$

In (11.45), (11.46), the term corresponding to $m = \pm 2, \pm 1$ becomes zero and only the term of (11.8) remains. Then,

$$\begin{aligned} \rho_{\mathrm{sd}}^{\uparrow}(k_z) &= \left| \int e^{ik_z z} V(r) \left( \frac{3}{2} \right)^{1/2} \varepsilon R(r) \frac{1}{\sqrt{12}} (r^2 - 3z^2) dv \right|^2 \\ &= \frac{3}{2} \varepsilon^2 \cdot \frac{4}{12} \left| \int e^{ik_z z} V(r) R(r) z^2 dv \right|^2 . \end{aligned} \tag{11.49}$$

Similarly,

$$\rho_{\mathrm{sd}}^{\downarrow}(k_z) = \left( 1 - \frac{3}{4} \varepsilon^2 \right)^2 \cdot \frac{4}{12} \left| \int e^{ik_z z} V(r) R(r) z^2 dv \right|^2 . \tag{11.50}$$

② $\boldsymbol{k} = (k_x, 0, 0)$ case. The electric current is perpendicular to the magnetization which corresponds to $\rho_{\perp}$. Since at $M/m = \pm 2$ and $0$ , $1/\tau \neq 0$ and at $m = \pm 1$, $1/\tau = 0$

$$\begin{aligned}\rho_{\mathrm{sd}}^{\uparrow}(k_x) &= \frac{3}{2}\varepsilon^2\left|\int e^{ik_x x}V(r)R(r)\frac{1}{\sqrt{12}}x^2dv\right|^2+\varepsilon^2\left|\int e^{ik_x x}V(r)R(r)\frac{1}{2\sqrt{2}}x^2dv\right|^2\\ &= \frac{3}{4}\varepsilon^2\frac{4}{12}\left|\int e^{ik_x x}V(r)R(r)x^2dv\right|^2.\end{aligned} \tag{11.51}$$

Also,

$$\begin{aligned}\rho_{\mathrm{sd}}^{\downarrow}(k_x) &= \left(1-\frac{1}{2}\varepsilon^2\right)^2\left|\int e^{ik_x x}V(r)R(r)\frac{1}{2\sqrt{2}}x^2dv\right|^2\\ &\quad+\left(1-\frac{3}{4}\varepsilon^2\right)^2\left|\int e^{ik_x x}V(r)R(r)\frac{1}{\sqrt{12}}x^2dv\right|^2\\ &\quad+\left|\int e^{ik_x x}V(r)R(r)\frac{1}{\sqrt{12}}x^2dv\right|^2\\ &= \left(1-\frac{3}{4}\varepsilon^2\right)\left|\int e^{ik_x x}V(r)R(r)x^2dv\right|^2.\end{aligned} \tag{11.52}$$

Therefore,

$$\frac{4}{12}\left|\int e^{ik_x x}V(r)R(r)x^2dv\right|^2=\frac{4}{12}\left|\int e^{ik_x x}V(r)R(r)z^2dv\right|^2\equiv\rho'.$$

Then,

$$\begin{aligned}\rho_{\mathrm{sd}}^{\uparrow}(k_z)&=\rho_{//}^{\uparrow}=\frac{3}{2}\varepsilon^2\rho'\\ \rho_{\mathrm{sd}}^{\downarrow}(k_z)&=\rho_{//}^{\downarrow}=\left(1-\frac{3}{2}\varepsilon^2\right)\rho'\\ \rho_{\mathrm{sd}}^{\uparrow}(k_x)&=\rho_{\perp}^{\uparrow}=\frac{3}{4}\varepsilon^2\rho'\\ \rho_{\mathrm{sd}}^{\downarrow}(k_x)&=\rho_{\perp}^{\downarrow}=\left(1-\frac{3}{4}\varepsilon^2\right)\rho'.\end{aligned} \tag{11.53}$$

From these equations,

$$\begin{aligned}\rho_{//}^{\uparrow}&\approx\rho_{\perp}^{\uparrow}+\gamma\rho_{\perp}^{\downarrow}\\ \rho_{//}^{\downarrow}&\approx\rho_{\perp}^{\downarrow}-\gamma\rho_{\perp}^{\downarrow}.\end{aligned} \tag{11.54}$$

Here, $\gamma\approx 3\varepsilon^2/4$. When the spin–orbit interaction is negligibly small, we can set $\gamma=0$ in (11.54). Then, $\rho_{//}^{\uparrow}=\rho_{\perp}^{\uparrow}$, $\rho_{//}^{\downarrow}=\rho_{\perp}^{\downarrow}$, and $\rho_{//}=\rho_{\perp}$. Namely, no anisotropic magnetoresistance occurs.

It is quite difficult to explain that the spin–orbit interaction causes the AMR experimentally. As one method, the dependence of $\Delta\rho/\rho_0$ on the magnetic moment is discussed. Figure 11.15 shows $\Delta\rho/\rho_0$ as a function of magnetic moment ($n_B$) for various kinds of alloys. In both bulk and thin film [13] cases,

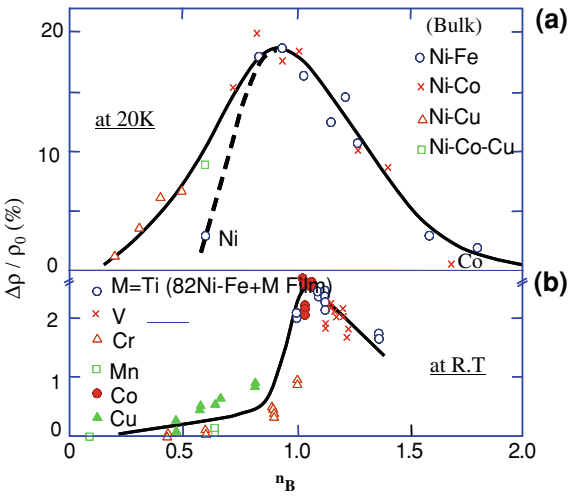


**Fig. 11.15** $\Delta\rho/\rho_0$ versus magnetic moment $n_B$

$\Delta\rho/\rho_0$ exhibits a maximum at around $n_B = 1$. It is concluded that the spin–orbital interaction works as a cause of the magnetoresistance effect because it is the most effective at $n_B = 1$.

## 11.6 Magnetoresistance Curve Based on the Magnetization Rotation Model

The strange shape of the magnetoresistance curve can be explained by simple calculation [14]. Moreover, the result might act as a practical use. The author introduces two examples for this. The directions of applied magnetic field $H$, saturation magnetization $M_s$, and the electric current now are taken with respect to the direction of the uniaxial anisotropy as shown in Fig. 11.16. The total energy of this system is,

$$E = K_u \sin^2 \beta - \mu_0 M_s H \cos(\theta - \beta). \tag{11.55}$$

We only have to calculate a component of magnetization in the direction of the applied magnetic field to draw the magnetization curve.

$$M = M_s \cos(\theta - \beta) \tag{11.56}$$

On the other hand, the magnetoresistance curve may be obtained only by calculating (11.57). $\rho_{//}$ and $\rho_\perp$ are electrical resistivities here when the magnetic field is applied in a parallel and perpendicular direction to the electric current direction, respectively. Here,$\rho_0$ is the one in the demagnetized state.

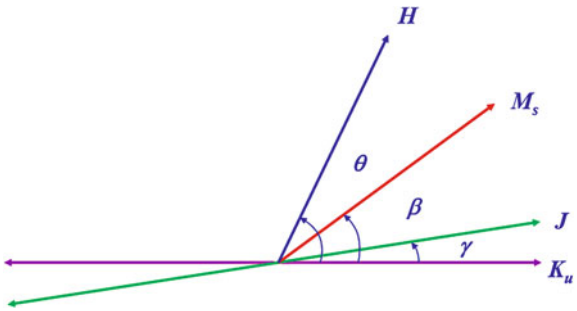


**Fig. 11.16** Coordinates when hysteresis curve and magnetoresistance curve are calculated

$$\frac{\rho_{//}-\rho_{\perp}}{\rho_0}=\frac{\rho_{//}-\rho_{\perp}}{\frac{\rho_{//}}{3}+\frac{2\rho_{\perp}}{3}}\left\{\cos^2(\gamma-\beta)-\frac{1}{3}\right\}. \tag{11.57}$$

Setting $M_s=1$, $\left(\rho_{//}-\rho_{\perp}\right)/\left(\rho_{//}/3+2\rho_{\perp}/3\right)$=1 and $H_k=2K_u/\mu_0 M_s$, we calculated the hysteresis curve and magnetoresistance curve (MR curve) when the direction of current is parallel to easy axis ($\gamma=0$). The result is shown in Fig. 11.17.

If the direction of the applied field deviates from the hard axis, sharp dips appear. If the current direction deviates from easy axis, there appears hysteresis in the MR curve which is not shown in the figure. The dips and hysteresis mentioned above have been considered due to Bulkhausen noise. But they appear even in the uniform rotation of magnetization. Let us show another example of an MR curve for a film which has perpendicular magnetic anisotropy. Figure 11.18a shows MR curves reported by Velu et al. [15] for Co/Au multilayers. This resistance was measured in the film plane by applying magnetic field perpendicular to the film plane. The MR curve was calculated by (11.57) with $\theta=0°$ and $\gamma=0°$in the coordinate system shown in Fig. 11.16. As a result, resistance was constant as a function of the applied field, which was quite different from the curve in Fig. 11.18a. Further, the MR curve was measured with the assumption that easy axis is declined from the normal to film. A very similar curve with Fig. 11.18a was obtained when $\theta=40°$, $\beta=0°$, $\gamma=130°$, $2K_u/M_s=4$ (Oe) and combined with the case $\theta=40°$, $\beta=0°$, $\gamma=50°$, $2K_u/M_s=6$ (Oe) The result is shown in Fig. 11.18b and the corresponding hysteresis curve in Fig. 11.18c. The calculated MR curve agrees well with that of experiment, supporting the propriety of the model described above. Although the measurement of magnetoresistance is very simple, we are able to investigate the magnetization process from the MR curves.

## 11.7 Giant Magnetoresistance Effect of Metallic Superlattices and Multilayer Films

The research on the metallic superlattice was from the end of 1970 to 1980. Judging from a historical point of view, the magnetic memory and the bubble magnetic memory, using the Permalloy thin film carried out ahead of this generation, were

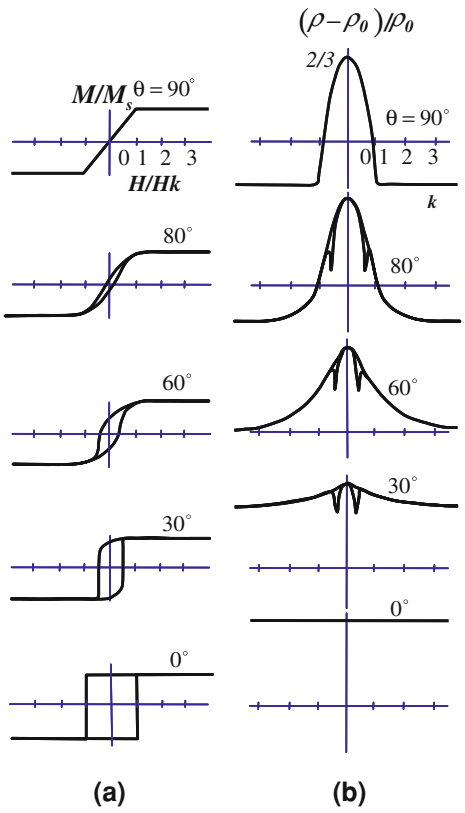


**Fig. 11.17** Examples of hysteresis curve (**a**) and magnetoresistance curve (**b**)

researched. It can be said that thin film preparation technology, microfabricating technology, and the characterization technique cultivated there enabled this research though those researches did not develop greatly. Especially, the MBE (molecular beam epitaxity) technology is a suitable multilayer film-making technology for the metallic artificial superlattice, and contribution to the superlattice research was developed remarkably. As for the research on the metallic superlattice, especially initial research, reports such as multilayers effective for the generation of the perpendicular magnetic anisotropy or the high saturation magnetization thin film were eagerly performed. Moreover, such researches were chiefly done in Japan. However, it might be a report on GMR of the Fe/Cr artificial lattice, after all, that drew a lot of researchers (magnetic) in thin film study to the field of the metallic artificial superlattice.

Figure 11.19 shows MOKE hysteresis loops measured along easy and hard axes and corresponding MR curves for GaAs(100)/12nmFe/1nmCr/12nmFe sandwich junction [16]. If we start with parallel alignment in the positive field direction and reduce $B_0$ (see Fig. 11.19a), then at a certain field the magnetization of one film reverses via domain wall motion (①). Hence in small fields we have antiparallel alignment. In such fields the corresponding resistance is high state (see Fig. 11.19c).

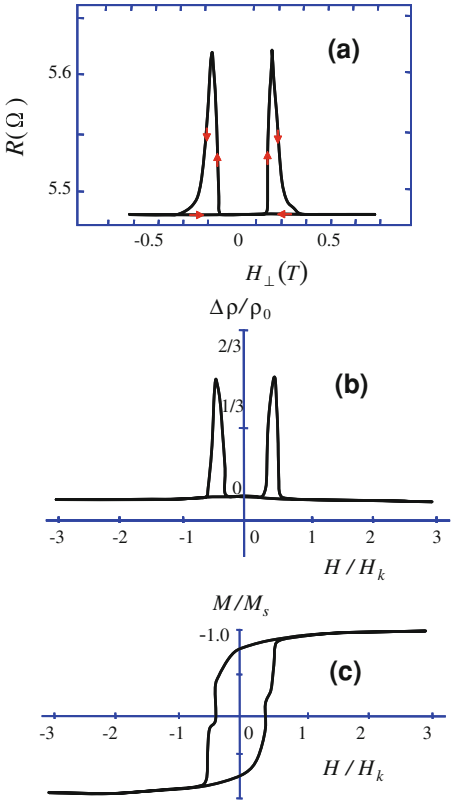


**Fig. 11.18** **a**Magnetoresistance curve for Au/Co(7.6Å)/Au(30Å)/Au measured at 4.2 K. **b** Calculated magnetoresistance curve and **c** corresponding hysteresis curve

In a negative field, at point ① in Fig. 11.19a, the other film also reverses and we have saturation. In this field, the corresponding resistance is low state (see Fig. 11.19c). In Fig. 11.19b MOKE loop measured along hard axis is shown and the corresponding resistance is shown in Fig. 11.19d. In this case we can also see that resistance is high at antiparallel state and low at parallel state. In Fig. 11.19d normal anisotropic magnetoresistance curve for a 250 Å thick film is also shown. The magnetoresistance ratio defined as $\left(R_{AP} - R_p\right)/R_P$ is one order larger than the anisotropic magnetoresistance of pure iron film.

Figure 11.20 shows the magnetoresistance curve of $(30\text{ÅFe}/9\text{ÅCr})_{40}$ superlattice [17]. The multilayered films can be made by MBE method for epitaxial growth on the GaAs(011).

Any of (a) and (b) in the curves of Fig. 11.20 are the magnetoresistance curves where the electric current is parallel and vertical to the applied magnetic field in plane of film, respectively. Curve (c) obtained in vertically applied magnetic field to the film plane corresponds to curves (a) and (b) corrected by the demagnetizing field. The point for which the shape of the magnetoresistance curve does not depend on the direction of the applied magnetic field is a feature of the GMR effect. When the mag-

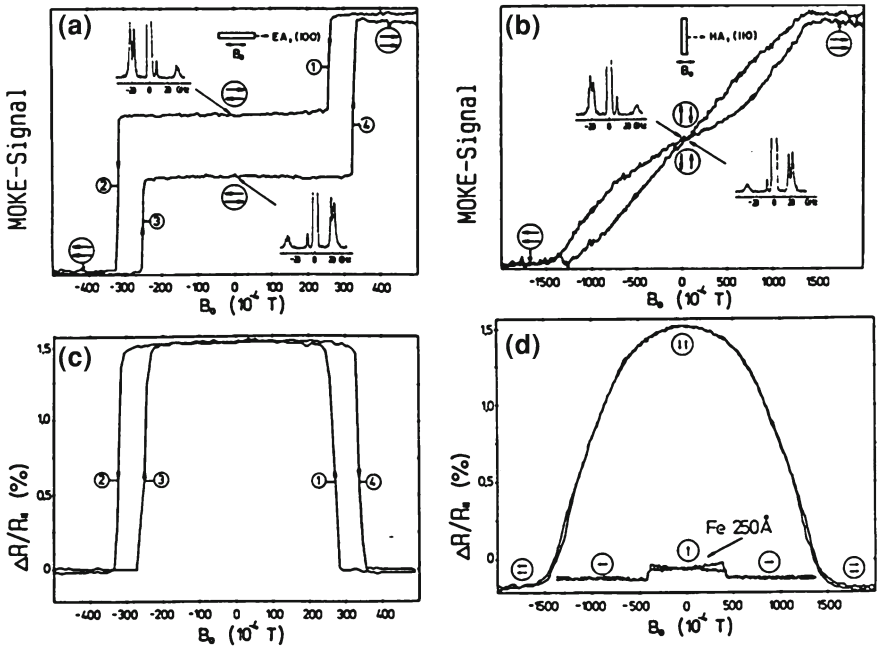


**Fig. 11.19** MOKE hysteresis curves (**a**, **b**) and magnetoresistance $\Delta R/R_{//} = \left(R - R_{//}\right)/R_{//}$ from Fe layers with anti-ferromagnetic coupling (**c**, **d**). Also, (**d**) displays the anisotropic MR effect of a 250 Å thick Fe film

**Fig. 11.20** Magnetoresistance curve of superlattices $(30\,\text{ÅFe}/9\,\text{ÅCr})_{40}$ (4.2 K)

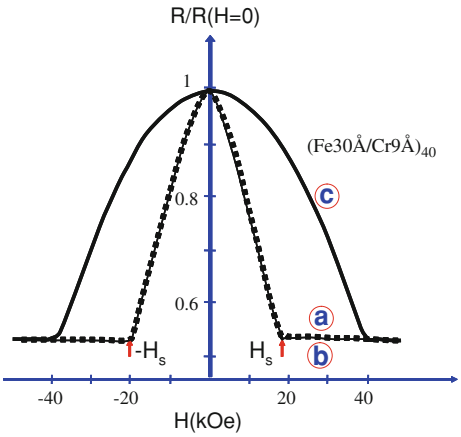


netic field is strong enough as shown in this figure, the magnetization of the Fe layer is saturated in the direction of the applied magnetic field and the magnetization of the layer interface becomes complete in parallel. On the other hand, an antiferromagnetic interaction works at the Fe layer interface without magnetic field. Consequently, the

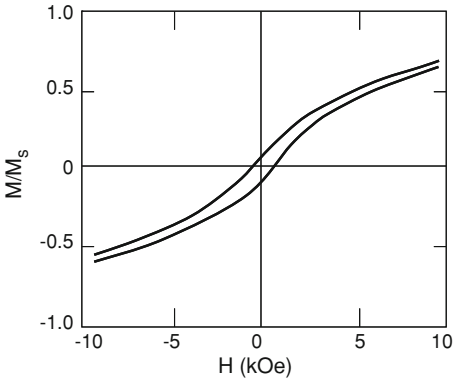


**Fig. 11.21** Magnetization curve of superlattice in Fig. 11.20

magnetization is in the state of an antiparallel. That is, when the magnetization of the layer interface is parallel, the resistance is small, but when it is antiparallel, the resistance is large. The magnetization curve in Fig. 11.21 corresponds to the magnetoresistance curve in Fig. 11.20. The antiferromagnetic interaction works through Cr at the Fe layer interface. This is confirmed by the experiment such as neutron scatterings. Moreover, it was shown that the interaction between the layer interfaces and the value of MR are correspondent excellently. In Fig. 11.22 one example is shown. Both the ratio of MR and the value of $H_s$ are corresponding to each other and, to be interesting, these oscillate with respect to the thickness of Cr [18]. Here, $H_s$ is the magnetic field where the magnetization is saturated in the magnetization curve and proportional to the magnetic interlayer interaction.

Later, the GMR effect and the interaction between magnetic interlayers of the combination of a lot of ferromagnetic substances and the non-magnetic substance including the Co/Cu multilayer film were researched. A phenomenological explanation of GMR has been discussed as much as AMR, etc. by the spin-dependent scattering (two-current model). That is, the electric current is assumed to bear independently with ↑ and ↓ spin electrons, and, in addition, the scattering with a spin flip is disregarded for easiness. The resistance $\rho_\uparrow$ and $\rho_\downarrow$ in $(F)$ parallel array of the magnetization of each ferromagnetic layer is given by $\rho_\uparrow = N\rho_+$ and $\rho_\downarrow = N\rho_-$, respectively. Here, $\rho_\uparrow$ and $\rho_\downarrow$ are resistance where 4s electrons are scattered, respectively by ↑ spin and ↓ spin of 3d band, and $N$ denotes the total interfaces. The total resistance is given by$1/\rho_F = 1/\rho_\uparrow + 1/\rho_\downarrow$. As the resistance of ↑spin and ↓spin is the same, $\rho_\uparrow = \rho_\downarrow = N\left(\rho_+ + \rho_-\right)/2$. From $1/\rho_{AP} = 1/\rho_\uparrow + 1/\rho_\downarrow = 2/\rho_\uparrow$, $\rho_{AP} = N\left(\rho_+ + \rho_-\right)/4$.

When we define the MR ratio as $\Delta\rho/\rho = \left(\rho_{AP} - \rho_P\right)/\rho_P$,

$$\frac{\Delta\rho}{\rho_0} = \frac{(\rho_+ - \rho_-)}{4\rho_+\rho_-} = \frac{(\alpha-1)^2}{4\alpha}. \tag{11.58}$$

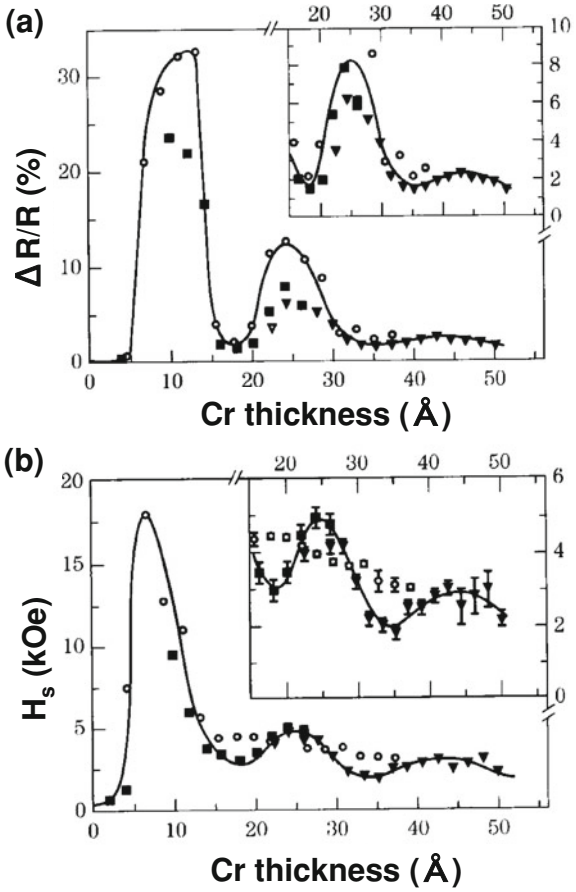


**Fig. 11.22** Cr thickness dependence of (**a**) MR ratio and (**b**) saturation magnetic field in Fe/Cr artificial lattice

is given. Therefore, it can be understood that GMR vanishes at $\alpha = 1$, that is, $\rho_+ = \rho_-$. Then, why is the spin-dependent scattering microscopically caused? The theories are roughly divided into two groups. One is by Inoue and Maekawa [19–21]. According to their theory, an irregular exchange potential due to the atomic mixing of the region of 1 and 2 atomic layers is mainly responsible for the phenomenon. The result of calculation according to this idea seems to explain the experimental result to some degree in Fig. 11.23 [22].

The other theory is by Edwards [23] that the principal cause may be the bulk scattering. If *d*band in the Fermi surface is remarkably different in ↑ spin and ↓ spins, it is expected that it is enough that scattering in the magnetic layer is different depending on the spin. When bands of Co and Ni are compared with that of Fe, the bulk scattering of the former is larger according to this idea. There are few examples

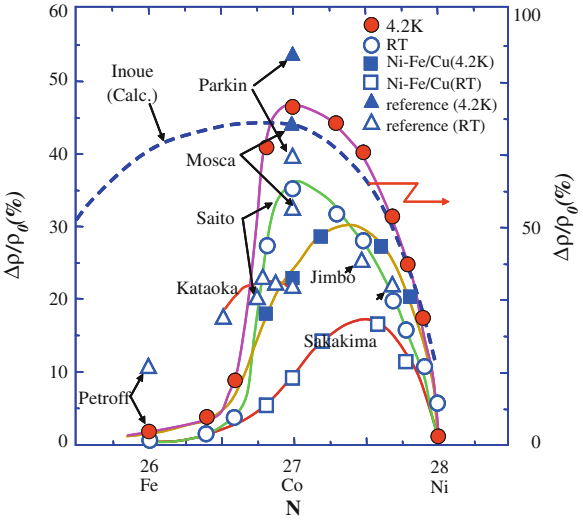


**Fig. 11.23** Electron concentration dependence of MR ratio of various artificial lattices

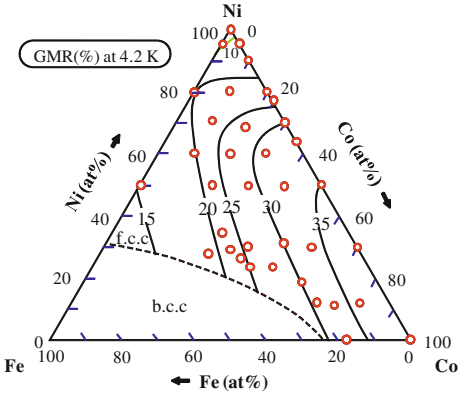


**Fig. 11.24** Composition dependence of GMR ratio of artificial lattice (15 ÅFe-Co-Ni/Cu)$_{30}$ (4.2 K)

of experimentally examining whether the interface scattering is effective or the bulk scattering is the main. The authors considered both the scatterings and explained the composition dependence of the GMR ratio of the Fe-Co-Ni/Cu multilayer film [24, 25]. One example is introduced here. In Fig. 11.24, the composition dependence of GMR ratio measured at 4.2 K of the multilayer films Fe-Co-Ni/Cu(15Å)/Cu (18-25Å) accumulated 30 times is shown in the contour line. The sample of the chemical composition of ◯ sign in the figure is made. According to the two-current model, the GMR ratio is by the above-mentioned (11.58). In $\alpha \equiv \rho_+/\rho_-$ of (11.4), $\rho_+(\rho_-)$ is a resistivity of ↑ spin (↓ spin) electrons that flow in the multilayer film. We assume it for the multilayer film as follows:

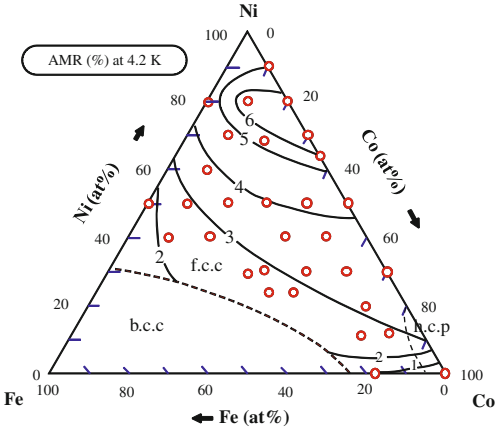


**Fig. 11.25** Composition dependence of AMR ratio of Fe–Co–Ni alloy thin film (4.2 K)

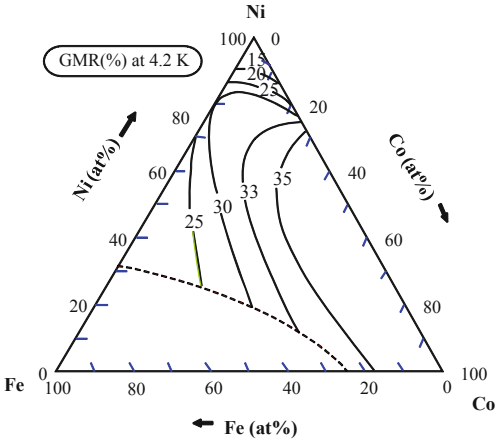


**Fig. 11.26** Composition dependence of MR ratio of $(Fe–Co–Ni/Cu)_{30}$ artificial lattice (calculated value)

$$\rho_\sigma = \rho_{\text{int}\,\sigma} + \rho_{\text{bulk}\,\sigma} + \rho_0 \quad (\sigma = + \text{ or } -), \tag{11.59}$$

where $\rho_{\text{int}\,\sigma}$, $\rho_{\text{bulk}\,\sigma}$, and $\rho_0$ mean the residual resistivity of the spin-dependent interface or bulk scattering in the multilayer film, and $\rho_0$ shows the residual resistivity that does not depend on the spin. The term $\rho_{\text{int}\,\sigma}$ is assumed to be given by the linear combination of the concentration of the M(Fe, Co, Ni) atom in the magnetic layer and the state density of the Fermi level of each diffusive magnetic impurity atom to Cu layer (calculated value). We can obtain $\rho_{\text{bulk}\,\sigma}$ by analyzing the composition dependence of AMR ratio shown in Fig. 11.25. In addition, $\rho_0$ is assumed to be changeable in proportion to the concentration of Fe. These values are substituted for (11.59) and, in addition, it is substituted for (11.4). As a result, we can obtain the composition dependence of GMR and the ratio of the interface on the bulk scattering (Fig. 11.26).

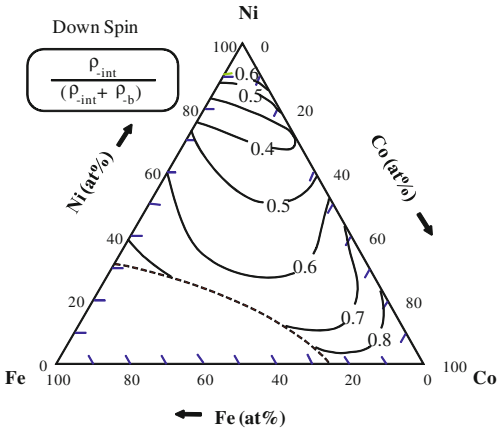


**Fig. 11.27** An interface scattering ratio of $\rho_{\downarrow}$

Figure 11.27 shows the interface scattering ratio of ↓ electron. As for ↑ electron, it is 0.4 in a core of the fcc region, and 0.6 in the circumference, and the composition dependence is not more remarkable than that of ↓ electrons. Moreover, when Figs. 11.26 and 11.27 are compared, it is understood that the magnetoresistance ratio is large in the chemical composition of rich Co where the interface scattering ratio of ↓ electron is large.

## References

1. S. Chikazumi, Kyouziseitai no buturi(II), p. 351 (1985). (Japanese)
2. W. Thomson, Proc. Roy. Soc. (London) **8**, 546 (1857)
3. T.R. Mcguire, R.I. Potter, IEEE Trans. Magn. **1**, 1018 (1975)
4. I.A. Campbell, A. Fert, O. Jaoul, J. Phys. C. Met. Phys. Suppl. 1. **S95** (1970)
5. S.von Molnar, S. Methfessel, J. Appl. Phys. **38**, 959 (1967)
6. I.A. Campbell, A. Fert, A.R. Pomeroy, Phil. Mag. **15**, 977 (1967)
7. A. Fert, I.A. Campbell, Phys. Rev. Lett. **21**, 1190 (1968)
8. A. Fert, I.A. Campbell, J. Phys, F. Metal Phys. **6**, 849 (1976)
9. O. Jaoul, I. A. Campbell, A. Fert, J. Magn. Magn. Mater. **5**, 23 (1977)
10. T. Miyazaki, M. Ajlma, J. Magn. Magn. Mater. **97**, 171 (1991)
11. T. Tatsumi, K. Yamada, Y. Kimura, H. Urai, J. Magn. Soc. Jpn. **1397**, 237 (1989)
12. I.A. Campbell, A. Fert, O. Jaoul, J. Phys. C. **3**, S95 (1970)
13. T. Miyazaki, M. Ajima, J. Magn. Magn. Mater. **81**, 91–95 (1989)
14. T. Miyazaki, M. Ajima, H. Sato, J. Magn. Soc. Jpn. **14**, 221 (1990)
15. E. Velli, C. Dupas, D. Renard, J.P. Renard, J. Seiden. Phys. Rev. B **37**, 668 (1988)
16. G. Binasch, P. Grunberg, F. Saurenbach, W. Zinn, Phys. Rev. B **39**, 4828 (1989)
17. M.N. Baihich. J.M. Broto, A. Fert, J. Nguyen Dau, F. Petroff, P.P. Etienne, G. Creuzet, A. Frieleich, J. Chazelas, Phys. Rev. Letts. **61**, 2472 (1988)
18. S.S.P. Parkin, N. More, K.P. Roche. Phys. Rev. Lett. **64**, 2304 (1990)
19. J. Inoue, S.Maekawa, J. Magn. Soc. Jpn. **16**, 623 (1992). (Japanese)
20. J. Inoue, A. Oguri, S. Maekawa, J. Phys. Soc. Jpn. **60**, 376 (1991)
21. H. Itoh, J. Inoue, S. Maekawa, Phys. Rev. B **4**, 5809 (1993)

22. H.Kubota, T.Miyazaki, J. Magn. Soc. Jpn. **18**, 335 (1994). (Japanese)
23. D.M. Edwards, J. Mathon, R.B. Muniz, IEEE Trans. Mag. **27**, 3548 (1991)
24. T. Miyazaki, J. Kondo, H. Kubota, J. Inoue, Appl. Phys. **81**(8), 5187 (1997)
25. H.Kubota, J.Kondo, T.Miyazaki, J. Inoue, J. Magn. Soc. Jpn. **21**, 561 (1997). (Japanese)